NEUROPHYSIOLOGY

Odontoblast TRPC5 channels signal cold pain in teeth

Laura Bernal[1,2]*, Pamela Sotelo-Hitschfeld[1,3]*, Christine König[1], Viktor Sinica[1,4], Amanda Wyatt[5], Zoltan Winter[1†], Alexander Hein[6‡], Filip Touska[1,4], Susanne Reinhardt[7], Aaron Tragl[1], Ricardo Kusuda[1§], Philipp Wartenberg[5], Allen Sclaroff[8], John D. Pfeifer[9], Fabien Ectors[10], Andreas Dahl[7], Marc Freichel[11], Viktorie Vlachova[4], Sebastian Brauchi[3,12], Carolina Roza[2], Ulrich Boehm[5], David E. Clapham[6‖¶], Jochen K. Lennerz[13¶], Katharina Zimmermann[1¶]

Teeth are composed of many tissues, covered by an inflexible and obdurate enamel. Unlike most other tissues, teeth become extremely cold sensitive when inflamed. The mechanisms of this cold sensation are not understood. Here, we clarify the molecular and cellular components of the dental cold sensing system and show that sensory transduction of cold stimuli in teeth requires odontoblasts. TRPC5 is a cold sensor in healthy teeth and, with TRPA1, is sufficient for cold sensing. The odontoblast appears as the direct site of TRPC5 cold transduction and provides a mechanism for prolonged cold sensing via TRPC5's relative sensitivity to intracellular calcium and lack of desensitization. Our data provide concrete functional evidence that equipping odontoblasts with the cold-sensor TRPC5 expands traditional odontoblast functions and renders it a previously unknown integral cellular component of the dental cold sensing system.

INTRODUCTION

Insults to the tooth's dentin produces inflammation, most commonly during tooth decay. Dental caries is a chronic disease in which a bacterial biofilm on the tooth surface, in combination with fermentable carbohydrate substrates, causes demineralization and eventually tooth decay. Worldwide, 2.4 billion people have untreated caries in permanent teeth (*1*). Inflamed teeth are extremely cold sensitive, perceived as a short, sharp intense neuralgic pain (*2*). On the basis of the functional anatomy, in which ceramic-like enamel and dentin insulate nociceptive terminals from temperature changes (*3*), the tooth pulp's sensory plexus of Raschkow is widely accepted as mechano- and nociceptive. In Brännström's hydrodynamic or fluid movement theory, the transduction of thermal and other physical stimuli to activate dentinal nerve endings has been attributed to a fluid dynamic–induced mechanosensory process. In this theory, dentinal microcanals (tubules) act as a hydraulic link between the physical stimulus and the nerve terminals, which are sited at the pulp-dentin boundary (fig. S1) (*4*). Functional experimental evidence for this theory is lacking.

The lack of functional evidence for cold sensing in teeth is unexpected given the progress in our understanding of molecular cold-sensing molecules (*5*). Certain transient receptor potential (TRP) ion channel subtypes are strongly activated by cooling, acting as molecular sensors in the skin and mucous membranes where they depolarize nerve terminals to elicit action potentials (*5*). In the skin, TRPM8 and TRPA1 act synergistically and represent the key sensors of environmental cooling as well as painful cold (*5*, *6*). TRPM8 and TRPA1 mRNA and protein are present in high density in the trigeminal ganglion (TG) and in the sensory axons of the tooth pulp (*7*–*9*). In addition, cultured human odontoblast-like cells (*10*) and cultured dental pulp fibroblasts (*11*) exhibit cold-induced increases in intracellular calcium in vitro, which is partly explained by their TRPA1 and TRPM8 channels. However, acutely isolated native human odontoblasts express TRPM8 but not TRPA1 (*12*), in contrast to these cells in more prolonged culture (*10*, *13*). In rat odontoblasts in vitro, cold sensitivity is controversial (*14*, *15*). The physiological significance of the observed cold transduction in odontoblast and fibroblasts is still unclear, because the specific contributions of TRPA1 and TRPM8 to cold-induced tooth pain in vivo were not observed (*16*) and electrophysiological models to directly examine the relevance of these channels in the tooth sensory system are missing. Thus, the cold transduction molecules and site of transduction in teeth remain unresolved.

We previously described that TRPC5 is cold sensitive in heterologous expression systems and its distribution in small- and medium-sized trigeminal and dorsal root ganglion neurons and the superficial laminae of the spinal dorsal horn is typical of sensors involved in temperature sensing and pain (*17*). Although TRPC5 is cold sensitive, no such function has yet been ascribed to TRPC5 in native cells. Here, we set out to understand the roles of TRPA1, TRPM8, and TRPC5 ion channels in cold sensing in teeth.

[1]Department of Anesthesiology, Erlangen University Hospital, Friedrich Alexander University of Erlangen-Nuremberg (FAU), Erlangen, Germany. [2]Departamento de Biología de Sistemas, Facultad de Medicina, Universidad de Alcalá, Alcalá de Henares, Madrid, Spain. [3]Institute of Physiology, Faculty of Medicine and Center for Interdisciplinary Studies on the Nervous System (CISNe), Universidad Austral de Chile, Valdivia, Chile. [4]Department of Cellular Neurophysiology, Institute of Physiology, Czech Academy of Sciences, Prague, Czech Republic. [5]Experimental Pharmacology, Center for Molecular Signaling (PZMS), Saarland University School of Medicine, Homburg, Germany. [6]HHMI, Cardiovascular Division, Boston Children's Hospital, and Department of Neurobiology, Harvard Medical School, Boston, MA, USA. [7]Center for Molecular and Cellular Bioengineering (CMCB), Technische Universität Dresden, Dresden, Germany. [8]Department of Otolaryngology, Washington University School of Medicine, St Louis, MO, USA. [9]Department of Pathology, Washington University School of Medicine, St Louis, MO, USA. [10]FARAH Mammalian Transgenics Platform, Liège University, Liège, Belgium. [11]Institute of Pharmacology, University of Heidelberg, Heidelberg, Germany. [12]Millennium Nucleus of Ion Channel-associated Diseases (MiNICAD), Santiago, Chile. [13]Center for Integrated Diagnostics, Department of Pathology, Massachusetts General Hospital/Harvard Medical School, Boston, MA, USA.
*These authors contributed equally to this work.
†Present address: Optical Imaging Centre Erlangen, Universität Erlangen-Nürnberg, Erlangen, Germany.
‡Present address: Department of Gynecology and Obstetrics, Erlangen University Hospital, Friedrich Alexander University of Erlangen-Nuremberg (FAU), Erlangen, Germany.
§On leave from: Departamento de Farmacologia, Faculdade de Medicina de Ribeirão Preto, Universidade de São Paulo, Ribeirão Preto, Brazil.
‖Present address: Janelia Research Campus, Howard Hughes Medical Institute, Ashburn, VA, USA.
¶Corresponding author. Email: claphamd@hhmi.org (D.E.C.); jlennerz@partners.org (J.K.L.); katharina.zimmermann@fau.de (K.Z.)

RESULTS

TRPC5 is required for inflammatory tooth pain

To evaluate cold transduction ion channels for inflammatory tooth pain, we first used an established dental pulp injury (DPI) model (*18*) in TRPC5, TRPA1, and TRPM8 null mice. A major sign of painful DPI in mice is a paradoxical increase in sucrose consumption (*18*). Administration of the anti-inflammatory analgesic indomethacin is sufficient to reverse the levels of sucrose consumption to that of uninjured controls (*18*). We found that DPI enhances the consumption of 5% room temperature sucrose water to ~3-fold above baseline (Fig. 1). In TRPA1$^{-/-}$ and TRPM8$^{-/-}$ mice, DPI induced a comparable increase in sucrose consumption. Notably, only in TRPC5$^{-/-}$ mice was sucrose consumption reversed to the level of the uninjured controls (Fig. 1), similar to the effect of indomethacin (*18*). These data indicate that cold-sensing TRPC5 is relevant and necessary for inflammatory tooth pain–associated behavior.

To enable functional examination of the entire tooth sensory system, we developed an intact mouse mandible-inferior alveolar nerve (jaw-nerve) preparation (Fig. 2). The ex vivo jaw-nerve preparation enables the recording of propagated action potentials from the inferior alveolar nerve to sensory stimuli in the mandibular incisor and molars, similar to recordings from nociceptors of the saphenous nerve with receptive fields in the skin (*6*). In contrast to the skin-nerve model in which recordings are made from finely split nerves (*19*), the inferior alveolar nerve in the jaw-nerve model is too short to enable these recordings. Therefore, we used a suction electrode to record voltage changes directly from the intact nerve end (Figs. 2 and 3A).

In this preparation, we focused on cold stimulation because it is adequate to produce tooth pain and activates the TRPC5 current in heterologous expression (*17*). When the intact jaw was exposed to cold, we observed large responses from ~10% of A- and C-fibers. Tooth cold receptor neurons fired 114 ± 15 action potentials per cold stimulus, with peak firing frequencies of 43 ± 5 per second. These values far exceed mouse skin nociceptor cold responses (16 ± 2 action potentials and firing frequencies of 3 ± 1 per second; Fig. 3, B and C). The thresholds of the tooth pulp nociceptors were 19 ± 1°C, 2°C lower than the cold nociceptors in the skin (cutaneous nociceptor threshold = 21 ± 1°C; Fig. 3D). There were no notable differences in cold responses between A- and C-fibers in these specific parameters (fig. S2).

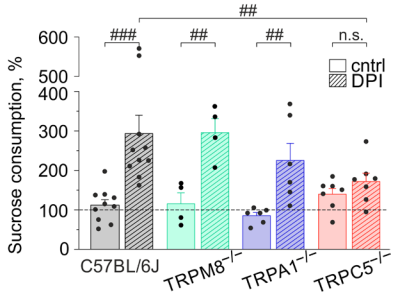

Fig. 1. TRPC5 is essential for inflammatory tooth pain. Percent change in sucrose consumption relative to baseline (dashed line) after DPI. DPI enhanced the consumption of 5% room temperature sucrose water to 293 ± 46% above baseline ($^{###}P$ = 0.00001). Lack of TRPC5 ($^{##}P$ = 0.005; 171 ± 21%), but not TRPM8 (P = 0.9; 299 ± 34%) or TRPA1 (P = 0.1; 225 ± 43%), reverts glucose consumption after DPI to baseline. The reduction in sucrose consumption in TRPC5$^{-/-}$ (n.s. P = 0.5), but not TRPA1$^{-/-}$ ($^{##}P$ = 0.006) or TRPM8$^{-/-}$ ($^{##}P$ = 0.004), was not different from the respective controls without DPI. n.s., not significant.

TRPC5 is a cold sensor in intact teeth

In the jaw-nerve preparation, the TRPC5 blockers HC-070 and ML204 effectively eliminated some tooth nociceptor's cold responses and, on average, reduced cold responses by 59 ± 13%. (Fig. 4, A and B). ML204, which also blocks TRPC4 and TRPC3 channels, had no effect in TRPC5$^{-/-}$ mice, suggesting that TRPC3 and TRPC4 were not involved as homomeric channels in cold responses. In addition, the TRPC5 agonist riluzole sensitized the cold response in TRPM8$^{-/-}$ jaws (fig. S3). In all fibers that remained unblocked by HC-070, the TRPA1 blocker HC-030031 abolished the remaining cold responses (97 ± 2%; Fig. 4, A and B). Furthermore, in the jaw-nerve preparations from TRPC5$^{-/-}$ mice, we found that the number of cold nociceptors was reduced by roughly half (Fig. 4C). We noted that although the remaining TRPC5$^{-/-}$ tooth nociceptors had unchanged response magnitudes, they had higher peak firing rates than any other strain (116 ± 34 action potentials, discharge rate of 66 ± 8 per second) and were activated at high threshold temperatures

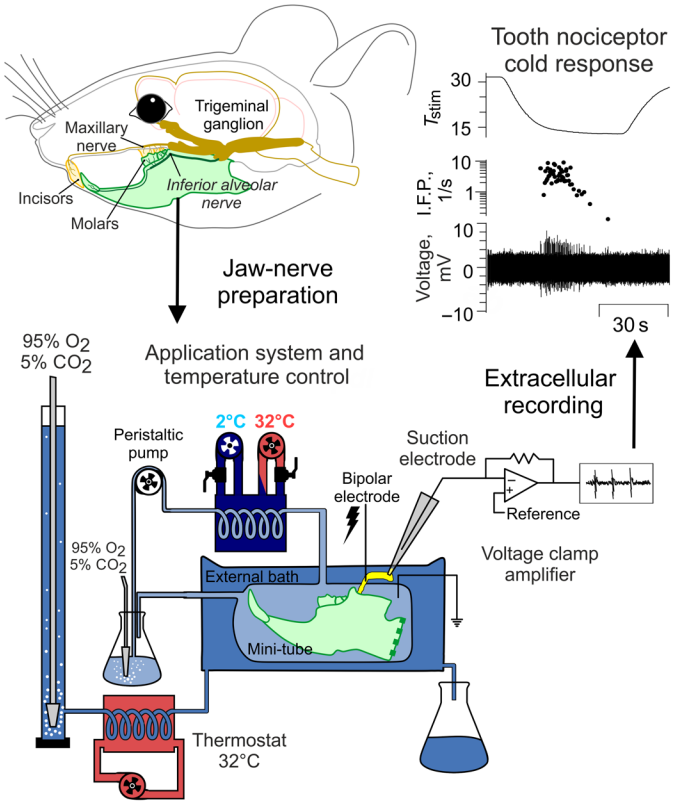

Fig. 2. Extracellular recordings from mouse tooth nociceptors in a novel jaw-nerve preparation. (**Top**) Illustration of mouse head with jaws and their innervation. The mandible-inferior alveolar nerve preparation is derived from the lower jaw and transferred to an organ bath consisting of an external solution and a mini-tube that is connected to a temperature-controlled application system. Connection of the application system's heating coil to a heating/cooling thermostat board permits rapid exchange of solution temperature in the mini-tube, where the preparation is exposed to chemical compounds and cold temperatures. Both the external and internal bath are supplied with oxygenized extracellular solution. Because of the short length of the inferior alveolar nerve, suction electrodes from glass capillaries are applied and the amplifier is used in a single-ended configuration. The external bath is required to prevent cold block in the nerve when the teeth in the mini-tube are exposed to cold. Action potentials from the inferior alveolar nerve are recorded in gap-free mode with Spike 2 (Materials and Methods).

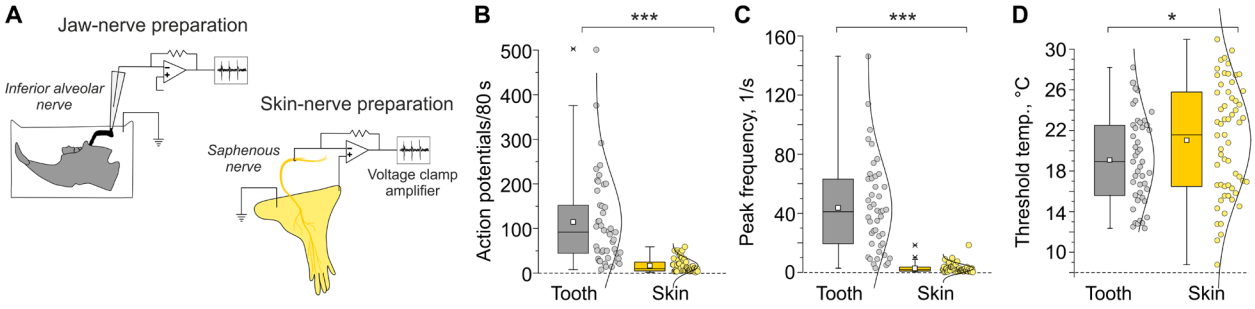

Fig. 3. Tooth nociceptor cold responses are much larger than skin cold nociceptor responses. (**A**) Schematic illustration of extracellular recordings from jaw-nerve as compared to skin-nerve preparations.(**B** to **D**) Comparison of the (B) cold response magnitude, (C) peak frequency, and (D) threshold temperature of C57BL/6J teeth ($n = 45$) and skin ($n = 59$) nociceptors. Statistical significance was identified by a two-sided Student's t test: $^{***}P = 2 \times 10^{-8}$, $^{***}P = 3 \times 10^{-11}$, and $^{*}P = 0.05$. Skin nociceptor cold responses are from (*6*, *50*) and refer to the same background strain at equivalent stimulus conditions.

(22 ± 1°C; Fig. 4, E to G). Although in mouse skin most of the cold responses are TRPM8-mediated (*6*), the teeth cold responses appeared insensitive to pharmacological TRPM8 modulation (fig. S4).

The deficits in the prevalence of TRPC5$^{-/-}$ cold responses, combined with the high efficacy of HC-070 and HC-030031 blockers, suggest that TRPC5 and TRPA1 are essential for cold sensing in teeth. In jaw-nerve preparations derived from TRPC5/A1-DKO (double-knockout) mice, we found that the number of cold responses was reduced by one-third (to <3%; Fig. 4C). Moreover, these cold responses had reduced response magnitudes and action potential firing rates compared to normal tooth nociceptors (20 ± 9 action potentials, discharge rate of 9 ± 3 per second) and were activated at very low temperatures (15 ± 1°C; Fig. 4, D to G). These small responses were insensitive to fast temperature drops (Fig. 4, D and H to J), and TRPM8 blockers or agonists had no effect (Fig. 4D).

We conclude that TRPC5 and TRPA1 are sufficient for cold transduction in healthy teeth. These findings raise the question of whether the specific anatomical context in teeth is required for TRPC5 cold sensitivity or if TRPC5 is also cold sensitive in the isolated cell bodies derived from the primary afferent terminals.

Dental primary afferent neurons (DPANs), the cell bodies of the sensory terminals in the maxillary plexus of Raschkow, are clustered in the cranial TG and were identified by retrograde labeling (*7*). Dissociated and in culture, they represent a model for the transduction processes in the tooth pulp's sensory nerves (fig. S5). We screened the red retro-labeled DPANs for cold-induced changes in [Ca^{2+}] and chemical responsiveness to the TRPM8 agonist menthol, the TRPA1 agonist carvacrol, the TRPC5 agonist riluzole, and the antagonist ML204. We identified ~17% of neurons as cold sensitive. Of these, 74% were sensitive to menthol and 57% to carvacrol, but only one neuron (<1%) was sensitized by the TRPC5 agonist riluzole (Fig. 5, A and B). Because menthol and carvacrol are not highly specific and can activate both TRPM8 and TRPA1, we also used DPANs derived from DKO strains, lacking TRPC5 and TRPM8 (TRPC5/M8-DKO) and TRPC5 and TRPA1 (TRPC5/A1-DKO). In DPANs derived from TRPC5/M8-DKO mice, we found that <5% of DPANs remained cold sensitive. These remaining DPANs were primarily sensitive to menthol and carvacrol, indicating activation of TRPA1 by cold. In DPANs derived from TRPC5/A1-DKO mice, 20% of cells were cold sensitive; of these, 75% were menthol sensitive and hence TRPM8 dependent (Fig. 5, A and C). These experiments imply that most of the DPANs use TRPM8 for cold responses, while few neurons rely on TRPA1 for independent cold responses. These observations match previous observations from dorsal root ganglion neurons (*20*).

Similar to DPANs derived from TRPC5/M8-DKO mice, DPANs from TRPM8/A1-DKO mice had few cold-sensitive cells (~5%) and none of these cells were activated by carvacrol or menthol (Fig. 5A). The TRPC5 blocker ML204 reduced their remaining cold-induced activity by 90% (Fig. 5, C and D). ML204's blocking effect was also found in the background strain (23% reduction), but absent in TRPC5$^{-/-}$ DPANs, where virtually all cold-sensitive DPANs were sensitive to menthol (93%; Fig. 5, A and D). In examining the cold-activated [Ca^{2+}] kinetics, TRPM8/A1-DKO DPAN signals were smaller and rose more slowly compared with the fast-rising response of menthol-sensitive neurons (fig. S6). To test whether total activity (approximated by the slope of the cold-activated [Ca^{2+}] signals) of the TRPM8/A1-DKO DPANs and riluzole-induced sensitization of the cold response represented functional TRPC5, we compared it to the responses of *mTrpc5* in human embryonic kidney (HEK) 293T cells and found both response patterns to be similar and riluzole to largely increase TRPC5 cold responses (fig. S6). In summary, nerve (DPAN) cold responses are dominated by TRPM8 with smaller and slower contributions by TRPC5 and TRPA1 channels.

TRPC5 cold transduction originates in odontoblasts

Consistent with the small number of nerve cells with functional TRPC5, a transcriptomic analysis from acutely dissociated labeled DPANs in the background strain identified *Trpm8* and *Trpa1*, while *Trpc5* was below the detection threshold (Fig. 6A and table S1). However, we visualized and quantified TRPC5 protein by multiphoton microscopy in retrograde-labeled whole TGs of reporter mice expressing tau-GFP (green fluorescent protein) under the control of the TRPC5 promoter (*21*). We focused on areas from the mandibular and maxillary branches that have the largest density of DPANs (*7*) and identified 3.5% TRPC5^{+} DPANs (Fig. 6B), similar to the 2.2 to 4.8% cold-sensitive, carvacrol- and menthol-insensitive DPANs in neuronal cultures from C57BL/6J or TRPM8/A1-DKO mice, respectively. In the cultured TRPC5^{+} trigeminal neurons from the TRPC5 reporter mice, we identified the typical doubly rectifying current-voltage relationship characteristic of TRPC5 (Fig. 6C). The current was small (chloride was eliminated from the solution to remove contaminating currents) and only detected after activation with Englerin (Fig. 6C). This small current was not modified by cold, suggesting modification of the properties of the native TRPC5 current by Englerin binding or by other factors. These findings

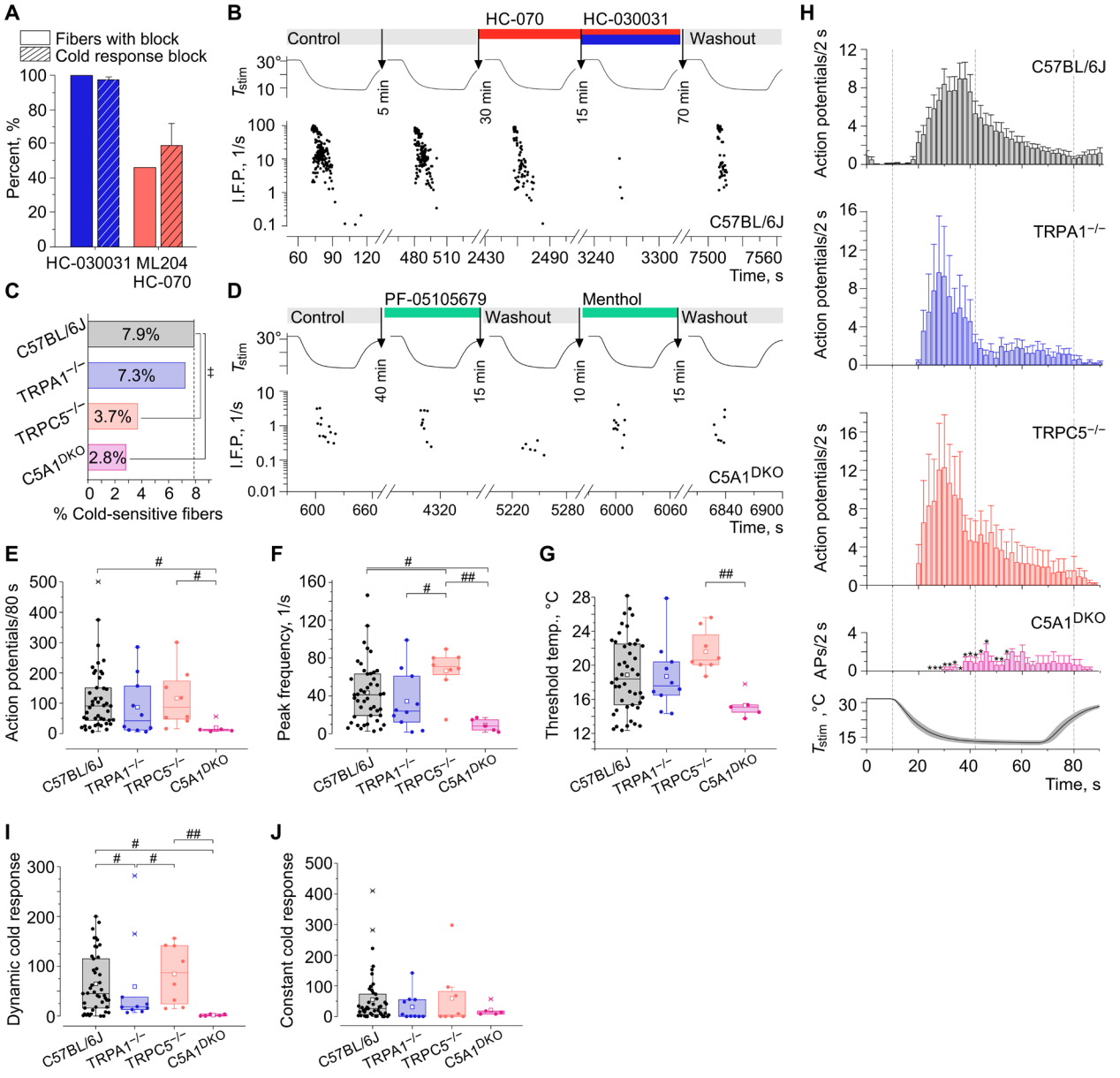

Fig. 4. TRPC5 and TRPA1 are sufficient as cold sensors in healthy teeth. (**A**) Percent cold-sensitive tooth nociceptors blocked by HC-030031 ($n = 9$ of 9 fibers) and ML204/HC-070 ($n = 6$ of 13 fibers) and respective fraction of block (means ± SEM). (**B**) C57BL/6J wt tooth nociceptor recording with temperature (top) and instantaneous frequency pattern (I.F.P.; bottom) blocked by HC-070 and HC-030031. Circles represent action potentials. (**C**) Tooth cold responses in TRPA1$^{-/-}$ ($n = 10$ of 138, $P = 1.0$), TRPC5$^{-/-}$ ($n = 8$ of 217, $^{‡}P = 0.04$), and TRPC5/A1-DKO ($n = 5$ of 177, $^{‡}P = 0.02$), chi-square tests versus C57BL/6J ($n = 45$ of 570). (**D**) Typical cold response of a TRPC5/A1-DKO tooth nociceptor with temperature (top) and instantaneous frequency pattern (I.F.P.; bottom). As in (B), circles represent action potentials, and horizontal bars and arrows indicate applications and respective time intervals. (**E** to **G**) Teeth nociceptor cold response characteristics according to genotype, (E) cold response magnitude [$P = 0.2$ between groups by one-way analysis of variance (ANOVA)], (F) peak firing frequency ($P = 0.01$), and (G) temperature threshold ($P = 0.06$). TRPC5/A1-DKO were statistically different from C57BL/6J wt ($^{#}P = 0.04$ and $^{#}P = 0.02$) and TRPC5$^{-/-}$ ($^{#}P = 0.05$, $^{##}P = 0.001$, and $^{##}P = 0.007$). TRPC5$^{-/-}$ were statistically different from TRPA1$^{-/-}$ ($^{#}P = 0.03$) and C57BL/6J ($^{#}P = 0.05$) in least significant difference post hoc tests. (**H** to **J**) Histograms in bins of 2 s (H) and respective box plots of (I) dynamic and (J) constant cold responses. Significant differences between groups by one-way ANOVA existed for dynamic (10 to 42 s of the histogram; $P = 0.01$) but not constant cold (44 to 80 s of the histogram; $P = 0.6$). TRPC5/A1-DKO ($n = 5$) and TRPA1$^{-/-}$ ($n = 10$) were different from C57BL/6J ($^{#}P = 0.02$ and $^{#}P = 0.03$, $n = 45$) and TRPC5$^{-/-}$ ($^{#}P = 0.01$ and $^{##}P = 0.02$, $n = 8$). Histograms present data as means ± SEM, and asterisks refer to two-sided Student's t test comparison of respective knockouts with the C57BL/6J background strain ($3 \times 10^{-6} < {}^{*}P < 0.002$). Lines represent medians, squares represent the mean, boxes represent the interquartile range (IQR), and whiskers represent 2.2-fold of IQR after exclusion of the >2.2 IQR outliers identified by crosses.

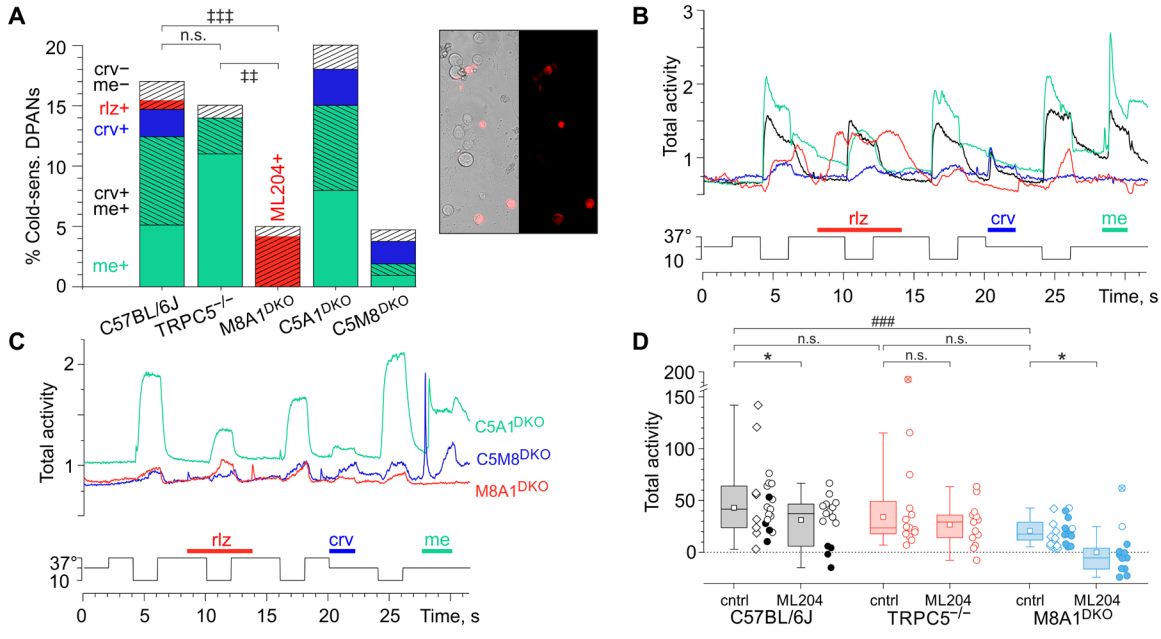

Fig. 5. Most cold-sensitive DPANs use TRPM8, but TRPA1 and TRPC5 are also functional cold transducers. (**A**) Characterization and quantification of cold-sensitive cultured DPANs (C57BL/6J: $n = 23$ of 136) based on Ca^{2+} transients measured with Fura-2 AM and sensitivity to TRP channel modulators menthol (me, $n = 7$), carvacrol (crv, $n = 3$), both ($n = 10$, descending diagonal stripes), neither ($n = 4$, ascending diagonal stripes), and riluzole (rlz, $n = 1$). Cold-sensitive DPANs insensitive to menthol and carvacrol (ascending diagonal stripes) are unchanged in TRPC5$^{-/-}$ ($n = 1$ of 14 in 93) versus C57BL/6J (3 of 23 in 136; n.s. $P = 0.86$), but increased in TRPM8A1-DKO ($n = 23$ in 457; $^{‡‡}P = 0.002$ and $^{‡‡‡}P = 0.00003$). In TRPC5A1-DKO, cold-sensitive cells ($n = 20$ of 100) were mostly menthol sensitive ($n = 15$; crv+ $n = 10$; both, $n = 7$ and none, $n = 2$). TRPC5M8-DKO cold-sensitive cells ($n = 5$ of 103) were mostly sensitive to carvacrol ($n = 3$; me+ $n = 2$; both, $n = 1$ and none, $n = 1$). Inset: Photomicrograph of cultured mouse TG neurons with red DiI retro-labeled DPANs. (**B** and **C**) Ca^{2+} transient traces from (B) C57BL/6J representative of four types of cold-sensitive neurons and (C) TRPM8A1-DKO (red), TRPC5A1-DKO (green), and TRPC5M8-DKO (blue). Bottom: Temperature stimulator command. (**D**) TRPM8/A1-DKO control (cntrl) cold responses ($n = 23$) were smaller than in C57BL/6J ($n = 23$; $^{###}P = 0.0007$) but not in TRPC5$^{-/-}$ neurons ($n = 13$; $P = 0.2$). ML204 (circles = treated neurons) blocked most cold responses in TRPM8/A1-DKO (≥50% block = filled circles, $n = 12$; $^{*}P = 0.01$) and some in C57BL/6J neurons ($n = 15$; $^{*}P = 0.02$), but not in TRPC5$^{-/-}$ neurons ($n = 13$; n.s. $P = 0.2$). n.s., not significant. Lines are medians, squares mean, boxes IQR, whiskers 2.2-fold IQR after exclusion of >2.2 IQR outliers identified by crosses.

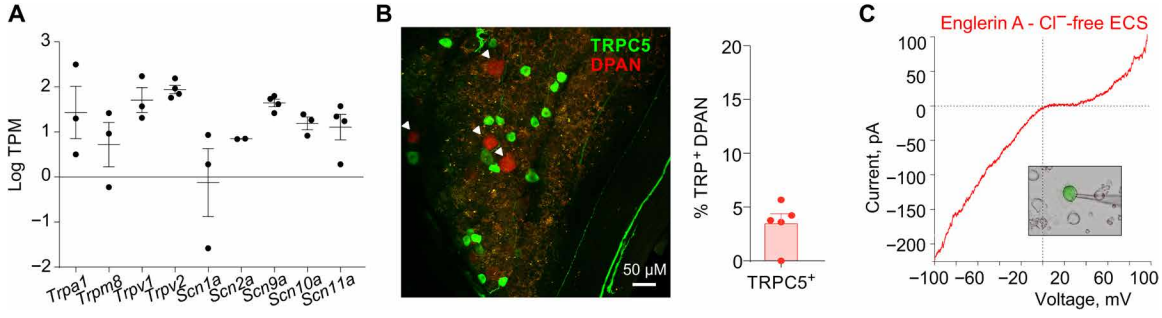

Fig. 6. Functional TRPC5 in trigeminal neurons. (**A**) Relative expression of TRP channel genes and nociceptor-specific subtypes of voltage-gated sodium channel genes in mouse DPANs given as transcripts per million (TPM). Data are presented as means ± SEM. Dots represent each replicate. Replicates with value 0 are not represented in the logarithmic scale. TRPC5 was not among the transcripts (see table S1). (**B**) Red DPANs (arrowheads) in TRPC5 reporter mouse ganglion (TG) multiphoton stacks of maxillo-mandibular regions. A total of 176 DPANs had 11 TRPC5^{+} neurons (seven TGs, five mice). (**C**) Typical doubly rectifying current-voltage relation observed in a cultured TRPC5^{+} neuron of a reporter mouse ($n = 13$). TRPC5 current is small and is only identified as Englerin-sensitized current subtracted from the baseline current in the absence of chloride in the solution.

demonstrate that TRPC5 is present in sensory neurons, although with healthy teeth TRPC5 cold responses are apparently small and rare.

What then accounts for the large TRPC5-mediated cold responses we observed in intact teeth? When we examined TRPC5 in reporter mice molar teeth, we found TRPC5 in practically all predentinal odontoblasts in the root-adjacent tooth pulp. The processes of the TRPC5-positive odontoblasts in dentinal tubules contacted sensory axons at the pulp-dentin boundary and ascended in tight association into the dentinal tubules. We did not identify TRPC5 in pulp fibroblasts or in sensory axons originating from the

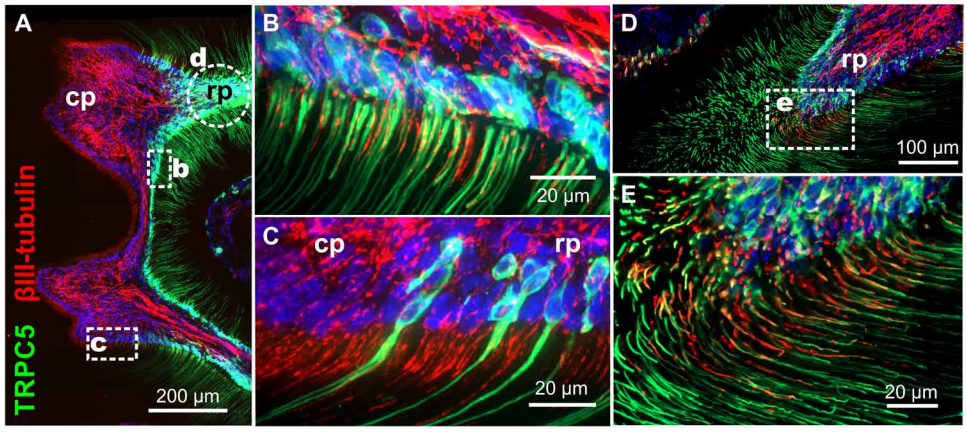

Fig. 7. TRPC5 channels are located in the odontoblast layer. (**A**) TRPC5 reporter mouse molar tooth whole mount with densely packed TRPC5$^+$ odontoblasts at the pulp-dentin boundary. (**B** and **C**) In tight association with sensory nerves. Green, TRPC5; red, βIII-tubulin; circle indicates area shown in (**D**) and (**E**) from a subsequent section. cp, coronal pulp; rp, radicular pulp. (E) Oblique section through the predentinal radicular pulp to visualize the tight association of TRPC5$^+$ odontoblast processes with their sensory nerves.

alveolar nerves and radiating through the root into the nerve plexus of Raschkow or in the inferior alveolar nerve (Fig. 7 and movies S1 and S2). Thus, TRPC5, in contrast to the ubiquity of TRPM8 and TRPA1 in anatomical compartments of mouse and human teeth (fig. S7) (*7*, *9*–*13*, *22*), is largely restricted to the odontoblast cell layer.

Ideally, TRPC5 should also be recorded in response to cold in odontoblasts in the intact tooth system of live, unanesthetized mice, but this has not yet been technically possible. Isolated odontoblasts do not fulfill this need because gene expression may be altered during isolation and culture. In addition, the respective functional phenotype depends on the origin of the cells, methods used for the induction of odontoblastic differentiation (*12*), developmental stage, intradental location, and innervation of the odontoblasts (*23*). A recent study, based on TRP channel expression patterns, implied that rat odontoblasts do not acquire potential sensory function before they begin to form root dentin (*24*). With these caveats in mind, we propose that TRPC5 expression and cold sensing indicate an essential sensory receptor function for the odontoblasts in the transduction hierarchy from the enamel to the dentinal primary afferent nerves.

TRPC5 is increased in human teeth with pulpitis

A remaining question is whether TRPC5 is also a cold sensor in human teeth and expressed in human odontoblasts and how it is affected in caries and inflammatory conditions associated with injured or patent pulp. In healthy human teeth from adults, removed for orthodontic or cosmetic reasons, we identified TRPC5 in the odontoblastic layer. We found more TRPC5 than TRPM8 in sensory nerves at the pulp-dentin boundary and in dentinal tubules. The sensors (*25*) at the pulpo-dentinal border zone (type II/III) exhibited the largest proportion of TRPC5 colabeling. In addition, we found a proportion of dentinal (type IV) TRPC5$^+$ fibers running within the dentinal tubules at the presumed site of sensory transduction (Fig. 8, A to E) (*26*).

Previous studies found that TRPM8 was decreased in axons of cold-hypersensitive human teeth (*22*). We thus directly compared TRPC5 with TRPM8 in inflamed human teeth with pulpitis (figs. S8 and S9) and found that TRPC5 sensory nerve expression markedly increased, while TRPM8 decreased. TRPC5 extended to the degenerating dentin and the entire tooth root, where we found a significantly higher percentage of TRPC5$^+$ pulp and root fibers (Fig. 8, F to I, and fig. S9). We also observed TRPC5$^+$ type IV fibers in the degenerating dentin (Fig. 8H). The higher percentage of TRPC5 in pulpitic teeth and the presence of dentinal fibers within the normal and degenerating dentinal tubules suggest that TRPC5 also acts as a cold sensor in human teeth.

DISCUSSION

Dentine sensitivity as a thermomechanical sensation

This study aimed to find the molecular cold-sensing mechanism in teeth. Using a novel jaw-nerve preparation that enabled us to record propagated electrical activity from intact teeth, we identified TRPC5 and TRPA1 as the molecular cold sensors and odontoblasts as the site of cold transduction. This experimental model allowed us to close an important gap in our understanding of tooth pain as it is the first model that allows the assessment of the tooth sensory system in its entire anatomical and, necessarily, physiological context in transgenic mice. This is critical because, unlike anywhere else in the body, the dental functional anatomy poses complex problems to sensing damaging physical stimuli. The odontoblast cellular layer's location in the outermost zone of the tooth pulp makes it a natural barrier between the mineralized hard tissues and the soft dental pulp. Each odontoblast has a process protruding in a dentinal tubule where it is immersed in dentinal fluid. Its cell body and process are surrounded by unmyelinated sensory nerves within the first 100 μm of the odontoblast-predentin border (fig. S1) (*26*). This unique hierarchical arrangement, from macroscale enamel via fluid-filled dentinal microtubules to molecular level ion channels, provides the structural basis for the encoding of thermal pain (*3*).

Previous theories of dentine sensitivity have interpreted tooth pain as the result of a thermomechanical sensory mechanism (*3*, *26*). The nerve theory suggests that the unmyelinated nerve fibers at the interface between predentin and dentinal tubules are the source of dentine sensitivity (*25*). However, the temperature at the pulp-dentin interface is still within the normal range when action potential trains are measured in tooth nerves (*27*) and when patients perceive pain from tooth cooling (*28*). This apparent inconsistency is resolved in Brännström's hydrodynamic theory, in which odontoblasts, with their

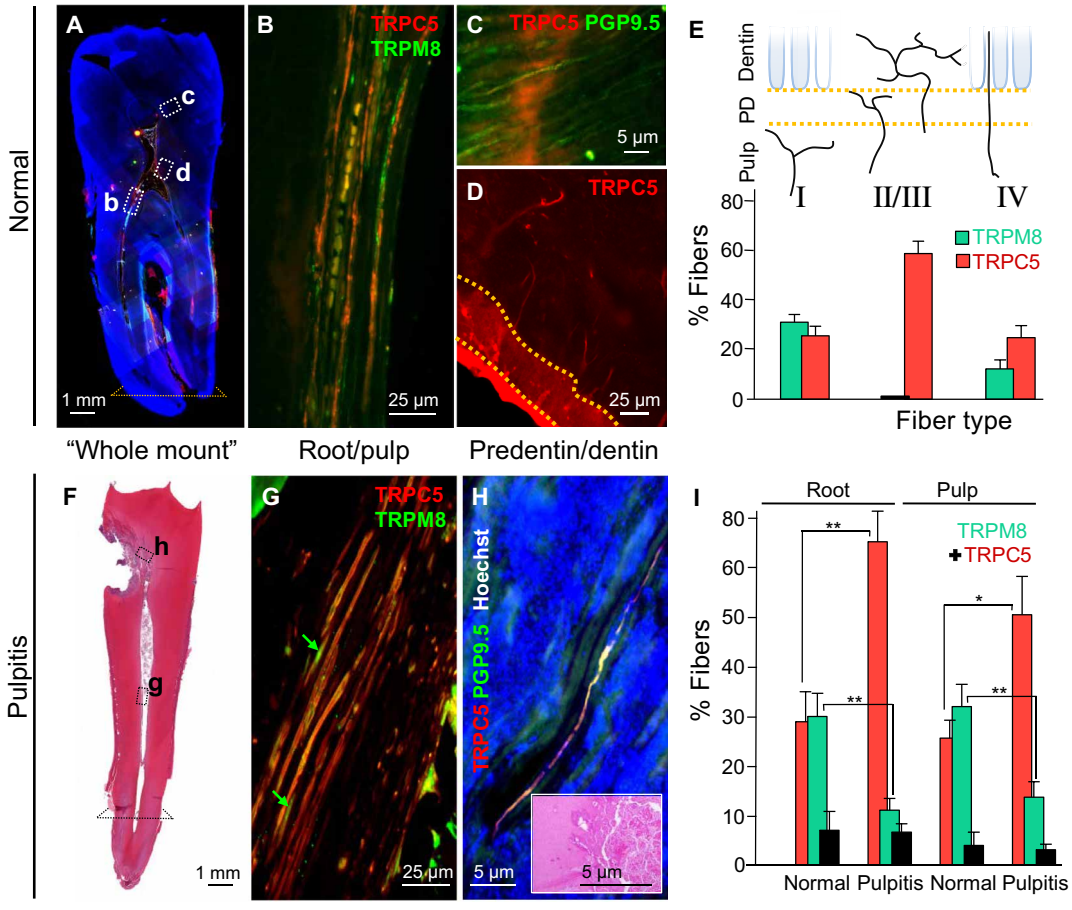

Fig. 8. TRPC5 is expressed in normal human teeth and increases with pulpitis. (**A**) Whole-mount panography of a human tooth; regions evaluated for TRPC5 expression are indicated; dotted line, level used in root measurement. (**B**) TRPC5$^+$ nerve fibers in the radicular pulp double labeled with TRPM8. (**C**) TRPC5$^+$ nerve fibers double labeled with PGP9.5 within the inner third of the dentinal tubules (type IV) ~40 µm above the odontoblast-predentinal border. (**D**) TRPC5$^+$ branched fibers (type II/III) in the predentin/dentin layer. (**E**) Quantification of TRPC5$^+$ and TRPM8$^+$ fiber types (four teeth). TRPC5/PGP9.5 and TRPM8/PGP9.5 for type I: 13/51 and 7/22; type II/III: 41/70 and 0/35; type IV: 26/105 and 6/49. (**F**) Hematoxylin and eosin (H&E)–stained human tooth whole mount with degenerated dentin (caries) and pulpitis. (**G**) Abundant TRPC5$^+$ and decreased TRPM8$^+$ (arrows) nerve fibers in the pulpitic tooth root. (**H**) TRPC5$^+$ nerve fibers (type IV) in degenerating dentin (inset, H&E). (**I**) Increased TRPC5$^+$ (190 of 660 versus 394 of 607 fibers; $^{**}P = 0.002$), decreased TRPM8$^+$ (197 of 660 versus 67 of 607; $^{**}P = 0.005$), and similar proportions of colabeled fibers (black) in normal versus pulpitic tooth roots [132 ± 78 ($n = 4$) versus 86 ± 21 ($n = 7$; $P = 0.2$)] and in the tooth pulp [TRPC5$^+$: 15 of 51 versus 81 of 161; $^{*}P = 0.01$; TRPM8$^+$: 622 of 161 versus 9 of 22; $^{**}P = 0.008$; colabeled fibers (black): 12 ± 3 ($n = 4$) versus 18 ± 8 ($n = 9$); $P = 0.3$]. Error bars, SEM.

associated sensory nerves at the pulp-dentine boundary, are assumed to be mechanosensory units for pain-evoking thermally induced hydraulic forces in the tubules (*4*, *26*). The tubule fluid has a greater coefficient of thermal expansion relative to the dentin matrix; thermal contraction and expansion of the dentinal fluid induces fluid movement (*29*). Flow-induced shearing was therefore considered as an adequate stimulus for molecular mechanoreceptors in the terminal nociceptor beads at the predentin-dentin interface. Although the rapid increase in cooling-induced outward-directed fluid flow observed in the dentinal tubules coincides with tooth pain and the intradental nerve discharge rate increases with increasing fluid flow (*27*, *29*), the theory is limited by lack of measurements and some inconsistencies. For example, etched dentinal tubules lead to dentine hypersensitivity but produce lower outward fluid flow in the tubules (*30*). Sealing the tubules then provides instant relief from cold hypersensitivity (*30*, *31*), but induces a larger cold-induced fluid flow (*30*). Humans with pulpal inflammation and painful cold hypersensitivity feel no pain from negative hydrostatic pressure on the tubules, despite the fact that it provokes equivalent outward fluid flow (*32*).

Last, some mechanical theories posit that the odontoblast processes are the initial mechanosensory nociceptors (*33*) based on the reasoning that odontoblast cells are more compliant relative to dentine and therefore would be expected to deform in registry with the tubules. The odontoblast transduction theory therefore hypothesizes that odontoblasts sense mechanical deformation and pass the signal to nearby nociceptors on nerve fibers through paracrine, electrical, or synaptic signaling (*3*, *33*). This transmission is implied by their close relationship to the nerve fibers but has not been observed ex vivo or in vivo.

Are physical forces in dentinal tubules sufficient to activate TRP channels?

Could TRPC5 act as multimodal transducer and respond to changes in macroscopic physical forces in addition to temperature? Enamel not only conducts temperature changes but also may expand or

contract when subjected to temperature changes (*3*, *29*). In primates, some of the odontoblast processes are "enamel spindles" (*26*) that span the boundary between enamel and dentin, where the two anisotropic materials may cause nonuniform temperature conduction. Property mismatch of bonded enamel and dentine leads to stress and flexure, even in the cause of a uniform change in temperature (*3*), causing friction and shear stress on the odontoblast processes.

TRPC5, like TRPA1 and TRPM8, channels are cold-activated in heterologous expression but, like all proteins, can potentially respond to primary physical forces. However, few TRP channels are subjected to these large forces in vivo (*34*) and only hTRPA1 has been shown to be gated by lipid-mediated forces, similar to Piezo channels (*35*). TRPC5 assembles with scaffolding proteins like EBP50 via cross-links between its VTTRL motif and the F-actin cytoskeleton, but deletion of TRPC5's C-terminal motif does not affect its membrane location or biophysical properties (*36*). Whether TRPC5 and TRPA1 are capable of recognizing shear stress in a compliant odontoblast or detect force changes of expanding and contracting enamel (*29*) is difficult to verify under physiologically relevant conditions. To date, all threshold mechanical forces found to open TRPC5 in cellular models [~2800 Pa; (*37*)] are many-fold larger than the forces in the dentinal tubules [~90 Pa provided from fitting predictions; (*3*)]. Proof of purely mechanically activated sensing because of temperature changes awaits the measurement of these forces at the site of the detector in vivo.

Odontoblasts are cold-transducing cells via TRPC5-mediated cold sensing

Here, we propose that the odontoblast processes—predominantly via TRPC5—are the initiating site of tooth cold transduction. The simplest interpretation of our data is that the observed restricted TRPC5 expression pattern, block of responses in genetically modified mice, and extracellularly recorded TRPC5 cold sensing indicate an essential sensory receptor function for the odontoblasts in tooth cold sensing.

More experiments are needed to clarify the functional relationship among odontoblasts, osteoblasts, and the tooth and between odontoblast processes and nerve endings. Some interesting observations may point the way. For example, the abovementioned enamel spindles cross the basement membrane of the enamel-dentine junction and may enable faster detection of temperature changes. For fast transmission, voltage-gated sodium currents in odontoblasts initiate rapid firing bursts similar to neurons (*38*). Axons produce bead-like swellings near odontoblasts with plasmalemmal appositions of 150 to 300 Å (*25*, *26*, *39*). Last, odontoblasts may couple to each other via gap junctions to act as a biological syncytium (*26*, *40*), and signal to axons via transmitters such as adenosine 5′-triphosphate (ATP), glutamate, or neuropeptides (*13*, *39*, *41*).

To summarize, our data clarify the molecular and cellular components of the dental cold sensing system and show that sensory transduction of cold stimuli in teeth requires odontoblasts. Thus, cultured neuron models alone are insufficient to capture the functional complexities of dental cold sensing. TRPC5 is a cold sensor in healthy teeth and, with TRPA1, is sufficient for cold sensing. Under human inflammatory conditions with injured or patent tooth pulp, TRPC5's expression increases in sensory axons. The odontoblast appears as the direct site of TRPC5 cold transduction and provides a mechanism for prolonged cold sensing via TRPC5's relative sensitivity to intracellular [Ca^{2+}] and lack of desensitization (*42*). TRPM8, in contrast, is down-regulated in inflammation and, with its contrasting biophysical properties and its location in the coronal predentinal odontoblasts of the enamel (*8*), may trigger more transient cold responses or indicate a different function (e.g., as an osmosensor akin to reports of TRPM8 in the cornea) (*43*). In addition to being an odontoblast cold sensor, TRPC5 may signal prolonged pain and act as a sensor of oxidative stress during inflammation (*44*). In this respect, TRPC5 may be an effective target for the treatment of dentin hypersensitivity and inflammatory tooth pain. Oil of cloves' (*Syzygium aromaticum*) main ingredient, eugenol, has been used for centuries as an analgesic in dentistry (*45*) and inhibits TRPC5 currents (fig. S10).

In the evolutionary arms race between teeth and food, the odontoblast with its elongated process stretching beyond the dentin-enamel boundary (*26*) satisfies the need for a specialized nociceptor inside an obdurate shell (*46*). We propose that odontoblasts alert us to tooth damage by extracorporeal, lower temperature, objects.

MATERIALS AND METHODS

Animal models and behavior

Animals

The animal ethics committee and the local district government of Middle Franconia, Germany approved the protocol for in vivo surgical interventions in mouse teeth under protocol no. 55.2-2532.1-9/14. Generation of the reporter strains was approved by the animal ethics committee and the local district government of Saarland, Germany under protocol no. 2.4.2.2-54/2015. We used adult male C57BL/6JCrl mice, congenic $TRPA1^{-/-}$ (*47*) congenic $TRPM8^{-/-}$ mice (*48*), and congenic $TRPC5^{-/-}$ mice (*49*). DKOs were generated from $TRPA1^{-/-}$ and $TRPC5^{-/-}$ mice, termed TRPC5/A1-DKO, from $TRPM8^{-/-}$ and $TRPA1^{-/-}$ mice, termed TRPM8/A1-DKO, and from $TRPC5^{-/-}$ and $TRPM8^{-/-}$ mice, termed TRPC5/M8-DKO. The TRPM8/A1-DKO mice were previously phenotyped for cold avoidance in the somatosensory system (*6*). Mice are specified in table S2. The animals were genotyped using the previously reported protocols (*49*–*51*). In addition, we generated reporter mouse lines to visualize TRPC5- and TRPA1-expressing cells by inserting an internal ribosome entry site (IRES) followed by a *Cre* recombinase complementary DNA (cDNA) downstream of the stop codon of the *Trpc5* (TRPC5-IC mice) (*21*) or the *Trpa1* gene, respectively (*52*). To generate the TRPA1 reporter mice, we produced an 8.7-kb targeting construct comprising a total of 5.2 kb of homologous sequence flanking an *IRES-Cre-PGK-Neomycin* cassette. The homologous stretches of DNA were generated by polymerase chain reaction (PCR), during which specific restriction sites were incorporated to enable assembly of the final construct by subsequent cloning steps. The *IRES-Cre-PGK-Neomycin* cassette is located 5 base pairs (bp) downstream of the stop codon, which is present in exon 27 of the *Trpa1* gene. After sequence verification, the targeting construct was electroporated into mouse embryonic stem cells. Correctly targeted stem cells were injected into blastocysts to generate the *Trpa1-IRES-Cre* (TRPA1-IC) knock-in mouse line. Flp recombinase deleter mice (*53*) were used to remove the neomycin resistance cassette. TRPC5-IC and TRPA1-IC mice were bred to *ROSA26*-floxed-stop tau GFP reporter mice (*54*) to label the TRPC5- or TRPA1-expressing cells with the microtubule-associated protein tau fused to GFP (tau GFP) (*52*). TRPC5-IC mice were genotyped using three primers

(*trpc5F*: tggcaggacatccgctattc, *trpc5R*: gggtcacctctgagaacagg, and *trpc5neoremF*: ccgtctctggtgtagctgatg) that produce two bands, 364 and 500 bp from the *wild type* (*wt*) allele and *IRES-Cre* alleles, respectively. Three primers were also used for the TRPA1-IC mice and produced bands of 460 and 264 bp for the *wt* and *IRES-Cre* alleles, respectively (*trpa1F*: gcacagttacctggtgcagaac, *trpa1R*: gggtgaggttgcaggaactagg, and *trpa1neoremF*: tccgtaacctggatagtgaaacagg). Mice were housed in an open cage facility in a 12-hour light-dark cycle according to the European Parliament Council (directive 2007/526/EG). All experiments accorded with the guidelines and regulations of animal care of the European Parliament Council (directive 2010/63EU) and the International Association for the Study of Pain Guidelines for the Use of Animals in Research.

Behavioral model of DPI and sucrose consumption

The experimental procedures were reproduced and then modified from Gibbs *et al.* (*18*). Female mice were used to be able to house them as adult mice in groups of four mice regardless of strain. Adaptation was performed in the home cage on two subsequent days where the mice were transferred to the experiment room at 8:00 a.m. and food and water were replaced by 5% sucrose until 5:00 p.m. Overnight, mice had free access to food and water. For the sucrose consumption measurement, the mice were weighed and then placed in individual cages without food and water for 7 hours. One hour before the measurement (3 hours before the beginning of the night phase), mice were transferred to the experimental room and water was replaced with individually prepared bottles filled with 5% freshly mixed sucrose solution (room temperature) and a charge-coupled device camera was centered on the bottle nipple of each cage. After 2 hours, the bottles were removed and weighed, and the animals transferred back to their group in the home cage. The amount of consumed glucose solution in 2 hours and the drinking attempts were analyzed from the video material to identify leaking bottles. Baseline sucrose consumption was assessed during two subsequent days. Animals needed to consume, on average, 0.4 ml to be included in the study. On the third day, animals were assigned to the control or DPI group. The DPI consisted of opening the pulp of the first and second maxillary molar with a dental burr during deep anesthesia (see DPAN surgery). The control animals were sham-treated by receiving anesthesia over a similar time, and the mouths were fixed open as during oral surgery in the DPI group. To reduce variability, all drilling was executed by the same experimenter. On the two subsequent days after the DPI or the sham operation, sucrose consumption was assessed after DPI and after sham treatment. The sucrose solution was prepared fresh every day, and the mice were weighed every day before the experiment. Raw data of sucrose consumption were subjected to an outlier analysis based on the interquartile range (IQR). The calculation of the quartiles and the statistical analysis was performed in SPSS 21 (IBM) using weighted average quartiles, and the outliers were excluded on the basis of the 2.2-fold IQR rule (*55*).

Electrophysiology

Jaw-nerve preparation and extracellular recordings

This new technique was developed to record from mouse tooth nociceptors. Animals were euthanized and beheaded, and the skin of the head was removed. The head was placed in a petri dish filled with synthetic interstitial fluid (SIF) and kept on an ice bed. SIF contained 108 mM NaCl, 3.5 mM KCl, 0.7 mM $MgSO_4$, 26.2 mM $NaHCO_3$, 1.7 mM NaH_2PO_4, 1.5 mM $CaCl_2$, 9.6 mM sodium gluconate, 5.6 mM glucose, and 7.6 mM sucrose. Mandibles were removed and cleaned from muscle, gingiva, and connective tissue, and the inferior alveolar nerve was exposed. The tooth pulp of incisor or molars was exposed to allow oxygen to diffuse, and part of the bone was removed to obtain an inferior alveolar nerve length of ~4 mm. The cleansed jaw-nerve preparations were kept refrigerated in oxygenated SIF until use. During the experiment, the jaw-nerve preparations were placed in a mini-tube and then in an organ bath chamber. The mini-tube was connected with the custom-built temperature control system, and the inferior alveolar nerve passed through a hole into the outer chamber. The jaw-nerve preparation was then continuously superfused with oxygenated SIF at a rate of 5 ml/min and maintained at 32°C by a thermostatic control system (Lauda Eco Silver E4 and Lauda ECO RE415). Electrophysiological recordings were made with suction microelectrodes pulled from borosilicate glass filaments (Sutter P-1000 Micropipette Puller) from the proximal end of the inferior alveolar nerve as previously described (*56*). An Olympus SZX7 microscope, micromanipulator (Märzhäuser MM 33), and custom-modified differential amplifier (EXT-02F, NPI Electronic GmbH) were used. The signal was recorded at 20 kHz with a Micro1401 MKII from CED (Cambridge Electronic Design) and analyzed offline with the Spike2 software (CED). Single nerve fibers were detected by electrical pulses delivered to the nerve trunk with a concentric bipolar electrode (no. CBJPL75, FHC Inc.). Electrical pulses of variable duration and intensity were applied to determine the threshold, and suprathreshold stimuli were applied (20- to 200-μs pulse width, maximum amplitude of 4000 mV) to visualize all fibers, present in the recorded filament. A previously described, custom-built countercurrent heat-exchange system (*19*) was adapted to apply 60-s cold stimuli (from 32° to 6°C) exclusively to the jaw-nerve preparation in the tube to avoid cold-induced block of conduction. Because of the experimental arrangement, the temperature could only be recorded at the outlet of the mini tube, ~1 cm away from the tooth. To obtain a better estimate of the temperature near the teeth, we made six temperature measurements between the two positions using two 0.05-mm-diameter ultrafast NiCr-Ni Type K thermoelements (#CHAL-002, Omega). We corrected the threshold temperatures of all cold responses individually with the adjusted temperature curve, taking into account the 4-s time difference and the −2.5°C offset. The difference amounted to ~6°C in threshold temperature. A cold response was defined as a discharge of more than two action potentials during the 60-s cooling periods before chemical stimulation. At least two control stimuli were performed before any pharmacological treatment was applied. Only fibers with reproducible cold responses were included in the pharmacological assessment. The time interval between subsequent cold stimuli was 5 min, and two to four subsequent cold stimuli were applied to register the baseline cold responsiveness. Fibers were classified according to their conduction velocity (CV) into A-fibers (CV > 1 m/s) or C-fibers (CV < 1 m/s). The peak discharge instantaneous frequency value was calculated as the average of at least two subsequent largest instantaneous frequency values. The temperature threshold of activation was determined as the temperature of the first action potential during cooling, and the magnitude of the response refers to the number of action potentials per 80-s cold stimulus (thus including rewarming). All compounds are specified in table S3.

Patch clamp recordings from acutely dissociated TG neurons

Recordings were made from TRPC5 reporter mice 1 to 3 days after plating. Whole-cell currents were recorded at a sampling rate of

10 kHz and low pass–filtered (eight-pole Bessel) at 2 kHz using an Axopatch 200B amplifier, Digidata 1440A digitizer, and pCLAMP 10 software (Molecular Devices). The patch electrodes were pulled from borosilicate glass with resistances between 3 and 6 megohms. Series resistance was compensated by >40% in all recordings. The voltages were corrected for the respective liquid junction potential of the chloride-free extracellular solution (ECS) (+3.4 mV). Background chloride currents resulted in a negative shift of E_{rev}; therefore, chloride-free (Cl^--free) solutions were used. Cl^--free ECS contained 145 mM Na isethionate, 1 mM $Mg(OH)_2$, 2 mM $Ca(OH)_2$, 10 mM Hepes, 10 mM glucose, and 5 mM 4-aminopyridine (4-AP), pH 7.4 adjusted with D-gluconic acid and osmolarity of 320 mOsm. Tetrodotoxin (1 μM) and the $Na_V1.8$ blocker PF-01247324 (1 μM) were added to the bath solution, prepared fresh from frozen stock on the day of experiment. The pipette solution contained 135 mM CsMES, 1 mM $MgCl_2$, 10 mM Hepes, 1 mM EGTA, 5 mM 4-AP, and 0.2 mM Na_2GTP, pH 7.4 adjusted with CsOH, osmolarity adjusted to 300 mOsm with glucose. The current-voltage relationships were recorded every 5 s using 500-ms linear voltage ramps from −100 to +100 mV (400 mV/s); holding potential was 0 mV. A combined automated fast solution changer with a double Peltier controller (CV Scientific) was used for drug application (Englerin A, 100 and 1000 nM). The Englerin-evoked currents were calculated by subtraction of currents recorded in the presence of Cl^--free ECS from the currents obtained in the presence of Englerin A. Englerin A was made fresh from frozen stock at the day of the experiment. Only one recording was performed from each cell culture dish to ensure that recordings were made from cells not previously exposed to chemicals.

Patch clamp recordings from HM1 cells

HEK293T cells stably expressing human muscarinic M1 receptor were maintained in Dulbecco's modified Eagle's medium (DMEM)/F12 (1:1), supplemented with 10% fetal bovine serum (FBS) and penicillin/streptomycin (10,000 U ml^{-1}) in 5% CO_2. C-terminal–tagged mouse TRPC5–enhanced GFP (EGFP) was transiently transfected using Lipofectamine 2000 (Invitrogen). Cells were recorded 24 to 48 hours after transfection. Recordings were performed at defined temperatures in ECS containing 140 mM NaCl, 5 mM KCl, 2 mM $CaCl_2$, 1 mM $MgCl_2$, 10 mM Hepes, and 10 mM glucose (adjusted to pH 7.4 with NaOH). The pipette (intracellular) solution contained 120 mM Cs-MES, 10 mM Cs_4-BAPTA, 10 mM Hepes, 2 mM Mg-ATP, 0.4 mM Na_2-GTP, 0.47 mM $MgCl_2$, and 3.26 mM $CaCl_2$. Whole-cell recordings were acquired at 5 kHz and low pass–filtered (8-pole Bessel) at 2 kHz. Capacity current was reduced using amplifier circuitry; series resistance compensation was set to 60 to 80%. Pipettes were heat-polished to a final resistance of 1.3 to 1.8 megohms.

Dental primary afferent neurons

Retrograde labeling of mouse DPANs

As previously published (*7*), molars were drilled with a dental burr and the carbocyanine dye (NeuroTrace, Thermo Fisher Scientific) was applied into the molar cavities. The holes were sealed with light-curable cement using a halogen 470-nm light source (750 mW/cm^2; Translux CL). All mice were anesthetized using a mixture of ketamine (90 mg/kg; Ketavet, Pharmacia GmbH) and xylazine (6 mg/kg; Rompun 2%, Bayer Vital GmbH) with eye protection. To prevent tooth inflammation and inflammatory pain from the procedure, animals were subcutaneously treated once a day with enrofloxacin (7.5 mg/kg Baytril 5%, Bayer Vital GmbH) and carprofen (4 mg/kg Rimadyl, Pfizer GmbH).

Calcium imaging of DPANs

Recordings were made from acutely dissociated TG neurons after retrograde labeling. Dissociated neurons were loaded with Fura-2 AM (Invitrogen, 3 μM supplemented with 0.02% pluronic dissolved in ECS) for 30 min and then washed for 15 min in ECS containing 145 mM NaCl, 5 mM KCl, 1 mM $MgCl_2$, 1.3 mM $CaCl_2$, 10 mM Hepes, and 10 mM glucose at pH 7.4. Calcium imaging experiments were made with an Olympus IX83 inverted microscope equipped with an Olympus UApoN340 20× water immersion objective. Fura-2 AM–loaded cells were excited with a 300-W xenon lamp (Lambda DG-4, Sutter Instrument) at 340 and 380 nm, and the emission was examined at 510 nm. An ORCA-Flash 4.0 LT digital camera (C11440, Hamamatsu Photonics) was used for image acquisition at a rate of 1 per second. Analysis was carried out with SlideBook 6 software (Intelligent Imaging Innovations). DiI-positive neurons were selected in the culture (excitation at 556 to 590 nm and examined at 602 to 664 nm). Cold stimulation of 10°C was realized with a combined automated fast solution changer with a double Peltier controller (CV Scientific). Menthol (500 μM), ML204 (100 μM), and KCl (145 mM) were applied during the measurement. Cold-induced activity of the fluorescence signal was computed as the area under the respective traces (120-s time frames). Cells were considered cold sensitive or sensitive to drugs (menthol, carvacrol, riluzole, ML204) when the averaged Ca^{2+} signal reached 2.5 × SD above the preceding baseline. All compounds are specified in table S3.

Multiphoton microscopy in retrograde-labeled mouse TG

Five days after surgery, mice were intracardially perfused with phosphate-buffered saline (PBS) and 4% paraformaldehyde (PFA) and the TGs were removed. TGs were left in PFA at 4°C for 6 hours. For staining with an anti-GFP antibody (table S4), the ganglia were pretreated with 100 μM digitonin according to a previously established protocol to preserve DiI from diffusion (*57*). The ganglia were mounted in agarose, and image stacks were acquired with a Zeiss LSM 880 NLO microscope equipped with a 680- to 1300-nm tunable and fixed 1040-nm two-photon laser (Newport Spectra-Physics) and a 20× W-Plan Apochromat objective lens. Fluorophores were excited at 1040 nm (DiI) and 920 nm (tau GFP), and fluorophore emissions were detected with nondescanned GaAsP detectors at 575 to 610 nm (DiI) and 500 to 550 nm (tau GFP). Fiji ImageJ was used to process the data, and the ImageJ Cell Counter plug-in was used to quantify cell numbers. For TGs, two different experimenters counted the cell bodies; the results represent their mean score.

RNA sequencing from DPANs

DPANs were selected from acutely dissociated TG cultures of C57BL/6JCrl mice, which were labeled as previously described with Neurotrace (*7*). After 3 days, the TGs were extracted, and cultures were obtained from dissociated neurons. Labeled cells were recognized and collected under an Olympus IX83 inverse microscope equipped with a vacuum-assisted single-cell collection device (Unipick, NeuroInDx). Four sets of red-labeled cells were selected, and 10 to 20 cells were pooled by transferring them to lysis buffer–containing tubes and stored on dry ice until subjecting them to transcriptomic analysis by the deep sequencing group at Technische Universität Dresden according to established protocols (*58*). Briefly, samples were amplified using single-cell exponential mRNA amplification service [SMARTer Ultra Low RNA Kit v2 (Clontech) or SMART-Seq2 (*59*)], further processed with a Nextera DNA library preparation kit (Illumina), and sequenced on Nextseq500 to depth between 15 and 20 million fragments per sample. The mapping was

performed with Genomic Short-read Nucleotide Alignment Program (GSNAP, v 2017-08-15) (*60*) using the mm10 reference genome and Ensembl 87. The expression levels were calculated using featureCounts (v1.5.3) (*61*). To allow a comparison of the sets, data are represented as transcripts per kilobase million (TPM) and displayed on a logarithmic scale.

Cell culture

Mouse TG culture

Cultures were performed as previously described (*7*). Five days after surgery, mice were euthanized, and the TGs were removed. For each experiment, ganglia of two or three animals were combined, transferred in sterile DMEM (Thermo Fisher Scientific), and fragmented. For cell dissociation, TG fragments were incubated in a mix of protease (Sigma-Aldrich; 1:2000) and collagenase (Sigma-Aldrich; 1:1000) in DMEM at 37°C and 5% CO_2 for 45 min. The cell suspension was then washed in DMEM and TNB 100 medium (Biochrom GmbH), supplemented with TNB 100 lipid-protein complex (Biochrom GmbH), streptomycin/penicillin (100 μg/ml; Thermo Fisher Scientific), and 1 nM nerve growth factor-7S (Alomone Labs), and cell clusters were triturated. Twenty microliters of cell suspension was applied per poly-D-lysine–coated FluoroDish (World Precision Instruments) and incubated in 1-ml TNB medium for 15 to 18 hours at 37°C and 5% CO_2.

HEK293T cell culture and transfection procedure

Cells were transiently transfected with mouse *Trpc5* cDNA as previously described (*17*, *42*), using Nanofectin (PAA Laboratories GmbH) according to the manufacturer's protocol. HEK293T cells were maintained in DMEM medium (Gibco Life Technologies) supplemented with 10% FBS, glucose (4.5 g/liter), and 1% penicillin/streptomycin. Cells plated on poly-D-lysine–coated coverslips were loaded with 3 μM Fura-2 AM (Invitrogen) supplemented with 0.02% pluronic acid (Invitrogen) for 30 min at 37°C and 5% CO_2 followed by a 15-min washout. Ratiometric calcium imaging of *mTRPC5* was performed 24 hours after transfection as described above.

Immunohistochemistry and histology

Immunohistochemistry in mouse molar tooth sections

Mice were intracardially perfused with PBS and 4% PFA, and the jaws were extracted and cleansed. For each genotype, tissues of two reporter mice were used. The jaws were left overnight in PFA at 4°C, then washed three times for 20 min in PBS at room temperature, and transferred to 20% EDTA for 24 hours at 37°C. We used S.C.E.M (Section Lab Co. Ltd.) and a small metal container immersed in hexane on dry ice at −77°C to embed the jaws. The frozen blocks were kept at −80°C and transferred to −20°C 6 hours before sectioning. The CryoJane Tape-Transfer System (CryoJane, Leica Microsystems, GmbH) was used to obtain serial sections of mouse molar teeth without distortion. Cryosectioning was performed (Leica CM3050) using adhesive tape applied to the frozen tissue block with a hand roller. The 16-μm-thick frozen sections were captured on tape, and the tape was rolled onto an adhesive glass slide (4× pretreated according to the manufacturer's instructions) and polymerized by ultraviolet-light irradiation into a plastic layer to anchor the frozen section to the glass slide. The tape was peeled off the section, and the section was subjected to immunohistochemical staining. The sections were blocked with 1% bovine serum albumin (BSA), 0.5% Triton X-100, and 5% goat serum in PBS at 4°C overnight, then incubated with antibodies diluted in 1% BSA and 0.5% Triton X-100 in PBS at 4°C overnight, and washed three times for 20 min in PBS. Subsequently, the sections were sealed with coverslips using a DAPI (4′,6-diamidino-2-phenylindole)–containing embedding medium. We visualized βIII-tubulin and amplified the GFP signal in reporter mice with antibodies listed in table S4. The sections were visualized using a Zeiss Spinning Disc Axio Observer Z1 microscope using a 25× or 63× objective lens with oil immersion. From selected areas, subsequent planes were acquired and the three-dimensional microscopy data were animated according to a previously published method (*62*).

Histology and microscopy of human tooth sections

Institutional approval was obtained for the use of human tissue samples (protocol 08-0209, Washington University, Department of Pathology).

Tissues and fixation. Extracted teeth were carefully stripped of periodontal, but not periapical, tissue and sectioned using a water-cooled diamond cutting wheel. For vertical sections, the plane was oriented toward the very tip of the root, slightly to the side of the apical foramen (typically offset 1 to 3 mm toward the crown). Split tooth segments were fixed for 2 days in phosphate-buffered 4% PFA solution (pH 7.4). Decalcification protocols included demineralization for 1 to 3 weeks in a solution of 14% hypochloric acid and polyvinylpyrrolidone 2, two commercial solutions consisting of 10% formaldehyde, 8% formic acid, and 1% methanol (Decalcifier I, Surgipath Medical Industries) as well as HCl and EDTA in water (Decalcifier II, Surgipath Medical Industries), or methyl methacrylate embedding according to established protocols (*63*). All human samples were formalin-fixed and paraffin-embedded; hematoxylin and eosin (H&E) stains were performed using routine protocols.

Immunohistochemistry. For detection of TRPC5, TRPM8, and other neuronal markers, sections were incubated with combinations of the antibodies listed in table S4 and visualized with appropriate secondary antibodies conjugated to Alexa 350, 488, 555, or 594 (1:500) in combination with Hoechst 33258 staining (blue).

Microscopy. For fluorescence microscopy, sections were viewed and quantified using a Zeiss Axiovert 200 inverted fluorescence microscope and an Olympus AX70 epi-fluorescence microscope. For low power fluorescence of tissues larger than the 4× field, complete visualization was achieved by overlaying 150 to 450 manually acquired 20× to 40× images in the channels appropriate for the secondary antibodies (panography). H&E-stained slides were viewed with an Olympus BX51 light microscope and, for whole-mount views, scanned on a Scanscope XT microscope (Aperio). Quantification of nerve fibers and neurons followed established protocols (*64*). Briefly, nerve fiber quantification was performed in cross- and longitudinal sections obtained just superior to the apical foramen; image processing was performed using ImageJ (v. 1.37v http://rsb.info.nih.gov/ij/) and Photoshop CS3 (Adobe Systems).

Histopathology. Pulpitis was defined as previously described (*65*). Briefly, hyperemia and blood vessel dilatation were typically seen in combination with at least focal disruption of the odontoblastic layer. Abundant serous exudate (as a result of increased vascular permeability), early neutrophils, or partial pulp necrosis were not a requirement for diagnosis of pulpitis, but frequently present. Teeth with previous endodontic treatment and extensive pulp necrosis extending to the apex were excluded from analysis.

Statistical analysis

We used a two-sided Student's *t* test, as indicated, for the comparison of dependent samples. Group comparisons were performed

using one-way analysis of variance (ANOVA) followed by the least significant difference (LSD) test for extracellular electrophysiology data and behavioral data and a Tukey test for calcium imaging analysis. Chi-square tests were used to compare observed frequencies of the different genotypes with the background strain. In most figures, significant differences are indicated with one symbol for $P < 0.05$, two for $P < 0.01$, and three for $P < 0.001$. We used asterisks (*) for the *t* test, hashtags (#) for one-sided ANOVA followed by the LSD or Tukey post hoc tests, and double daggers (‡) for the chi-square test. Raw data were analyzed for outliers using the 2.2-fold IQR (*55*) from weighted average quartiles calculated in SPSS 21, and then box plot graphs were computed in Origin 2017.

SUPPLEMENTARY MATERIALS

Supplementary material for this article is available at http://advances.sciencemag.org/cgi/content/full/7/13/eabf5567/DC1

View/request a protocol for this paper from *Bio-protocol*.

REFERENCES AND NOTES

1. N. J. Kassebaum, E. Bernabé, M. Dahiya, B. Bhandari, C. J. L. Murray, W. Marcenes, Global burden of untreated caries: A systematic review and metaregression. *J. Dent. Res.* **94**, 650–658 (2015).
2. R. A. Alghaithy, A. J. E. Qualtrough, Pulp sensibility and vitality tests for diagnosing pulpal health in permanent teeth: A critical review. *Int. Endod. J.* **50**, 135–142 (2017).
3. M. Lin, G. M. Genin, F. Xu, T. Lu, Thermal pain in teeth: Electrophysiology governed by thermomechanics. *Appl. Mech. Rev.* **66**, 0308011–3080114 (2014).
4. M. Brännström, G. Johnson, Movements of the dentine and pulp liquids on application of thermal stimuli. An in vitro study. *Acta Odontol. Scand.* **28**, 59–70 (1970).
5. J. Vriens, B. Nilius, T. Voets, Peripheral thermosensation in mammals. *Nat. Rev. Neurosci.* **15**, 573–589 (2014).
6. Z. Winter, P. Gruschwitz, S. Eger, F. Touska, K. Zimmermann, Cold temperature encoding by cutaneous TRPA1 and TRPM8-carrying fibers in the mouse. *Front. Mol. Neurosci.* **10**, 209 (2017).
7. A. Kadala, P. Sotelo-Hitschfeld, Z. Ahmad, P. Tripal, B. Schmid, A. Mueller, L. Bernal, Z. Winter, S. Brauchi, U. Lohbauer, K. Messlinger, J. K. Lennerz, K. Zimmermann, Fluorescent labeling and 2-photon imaging of mouse tooth pulp nociceptors. *J. Dent. Res.* **97**, 460–466 (2018).
8. Y. S. Kim, T. H. Kim, D. D. McKemy, Y. C. Bae, Expression of vesicular glutamate transporters in transient receptor potential melastatin 8 (TRPM8)-positive dental afferents in the mouse. *Neuroscience* **303**, 378–388 (2015).
9. Y. S. Kim, H. K. Jung, T. K. Kwon, C. S. Kim, J. H. Cho, D. K. Ahn, Y. C. Bae, Expression of transient receptor potential ankyrin 1 in human dental pulp. *J. Endod.* **38**, 1087–1092 (2012).
10. I. A. El Karim, G. J. Linden, T. M. Curtis, I. About, M. K. McGahon, C. R. Irwin, F. T. Lundy, Human odontoblasts express functional thermo-sensitive TRP channels: Implications for dentin sensitivity. *Pain* **152**, 2211–2223 (2011).
11. I. A. El Karim, G. J. Linden, T. M. Curtis, I. About, M. K. McGahon, C. R. Irwin, S. A. Killough, F. T. Lundy, Human dental pulp fibroblasts express the "cold-sensing" transient receptor potential channels TRPA1 and TRPM8. *J. Endod.* **37**, 473–478 (2011).
12. K. Tazawa, H. Ikeda, N. Kawashima, T. Okiji, Transient receptor potential melastatin (TRPM) 8 is expressed in freshly isolated native human odontoblasts. *Arch. Oral Biol.* **75**, 55–61 (2017).
13. O. Egbuniwe, S. Grover, A. K. Duggal, A. Mavroudis, M. Yazdi, T. Renton, L. Di Silvio, A. D. Grant, TRPA1 and TRPV4 activation in human odontoblasts stimulates ATP release. *J. Dent. Res.* **93**, 911–917 (2014).
14. K. Y. Yeon, G. Chung, M. S. Shin, S. J. Jung, J. S. Kim, S. B. Oh, Adult rat odontoblasts lack noxious thermal sensitivity. *J. Dent. Res.* **88**, 328–332 (2009).
15. M. Tsumura, U. Sobhan, M. Sato, M. Shimada, A. Nishiyama, A. Kawaguchi, M. Soya, H. Kuroda, M. Tazaki, Y. Shibukawa, Functional expression of TRPM8 and TRPA1 channels in rat odontoblasts. *PLOS ONE* **8**, e82233 (2013).
16. B. Michot, C. S. Lee, J. L. Gibbs, TRPM8 and TRPA1 do not contribute to dental pulp sensitivity to cold. *Sci. Rep.* **8**, 13198 (2018).
17. K. Zimmermann, J. K. Lennerz, A. Hein, A. S. Link, J. S. Kaczmarek, M. Delling, S. Uysal, J. D. Pfeifer, A. Riccio, D. E. Clapham, Transient receptor potential cation channel, subfamily C, member 5 (TRPC5) is a cold-transducer in the peripheral nervous system. *Proc. Natl. Acad. Sci. U.S.A.* **108**, 18114–18119 (2011).
18. J. L. Gibbs, R. Urban, A. I. Basbaum, Paradoxical surrogate markers of dental injury-induced pain in the mouse. *Pain* **154**, 1358–1367 (2013).
19. K. Zimmermann, A. Hein, U. Hager, J. S. Kaczmarek, B. P. Turnquist, D. E. Clapham, P. W. Reeh, Phenotyping sensory nerve endings in vitro in the mouse. *Nat. Protoc.* **4**, 174–196 (2009).
20. T. Memon, K. Chase, L. S. Leavitt, B. M. Olivera, R. W. Teichert, TRPA1 expression levels and excitability brake by K_V channels influence cold sensitivity of TRPA1-expressing neurons. *Neuroscience* **353**, 76–86 (2017).
21. Y. Schwarz, K. Oleinikov, B. Schindeldecker, A. Wyatt, P. Weißgerber, V. Flockerzi, U. Boehm, M. Freichel, D. Bruns, TRPC channels regulate Ca^{2+}-signaling and short-term plasticity of fast glutamatergic synapses. *PLOS Biol.* **17**, e3000445 (2019).
22. L. T. Alvarado, G. M. Perry, K. M. Hargreaves, M. A. Henry, TRPM8 Axonal expression is decreased in painful human teeth with irreversible pulpitis and cold hyperalgesia. *J. Endod.* **33**, 1167–1171 (2007).
23. M. R. Byers, R. E. Westenbroek, Odontoblasts in developing, mature and ageing rat teeth have multiple phenotypes that variably express all nine voltage-gated sodium channels. *Arch. Oral Biol.* **56**, 1199–1220 (2011).
24. A. Tanaka, Y. Shibukawa, M. Yamamoto, S. Abe, H. Yamamoto, S. Shintani, Developmental studies on the acquisition of perception conducting pathways via TRP channels in rat molar odontoblasts using immunohistochemistry and RT-qPCR. *Anat. Sci. Int.* **95**, 251–257 (2020).
25. T. Gunji, Morphological research on the sensitivity of dentin. *Arch. Histol. Jpn.* **45**, 45–67 (1982).
26. C. F. Cox, K. Suzuki, H. Yamaguchi, J. D. Ruby, S. Suzuki, N. Akimoto, N. Maeda, Y. Momoi, Sensory mechanisms in dentine: A literature review of light microscopy (LM), transmission microscopy (TEM), scanning microscopy (SEM) & electro physiological (EP) tooth sensitivity: Is the ciliary organelle on the odontoblast the elusive primary nociceptor? *Dent. Oral Craniofacial Res.* **4**, 1–14 (2017).
27. N. Vongsavan, B. Matthews, The relationship between the discharge of intradental nerves and the rate of fluid flow through dentine in the cat. *Arch. Oral Biol.* **52**, 640–647 (2007).
28. H. O. Trowbridge, M. Franks, E. Korostoff, R. Emling, Sensory response to thermal stimulation in human teeth. *J. Endod.* **6**, 405–412 (1980).
29. P. Linsuwanont, J. E. Palamara, H. H. Messer, An investigation of thermal stimulation in intact teeth. *Arch. Oral Biol.* **52**, 218–227 (2007).
30. W. Chidchuangchai, N. Vongsavan, B. Matthews, Sensory transduction mechanisms responsible for pain caused by cold stimulation of dentine in man. *Arch. Oral Biol.* **52**, 154–160 (2007).
31. K. B. Muzzin, R. Johnson, Effects of potassium oxalate on dentin hypersensitivity in vivo. *J. Periodontol.* **60**, 151–158 (1989).
32. O. Ajcharanukul, W. Chidchuangchai, P. Charoenlarp, N. Vongsavan, B. Matthews, Sensory transduction in human teeth with inflamed pulps. *J. Dent. Res.* **90**, 678–682 (2011).
33. H. Magloire, M. L. Couble, B. Thivichon-Prince, J. C. Maurin, F. Bleicher, Odontoblast: A mechano-sensory cell. *J. Exp. Zool. B Mol. Dev. Evol.* **312B**, 416–424 (2009).
34. Y. A. Nikolaev, C. D. Cox, P. Ridone, P. R. Rohde, J. F. Cordero-Morales, V. Vasquez, D. R. Laver, B. Martinac, Mammalian TRP ion channels are insensitive to membrane stretch. *J. Cell Sci.* **132**, jcs238360 (2019).
35. L. Moparthi, P. M. Zygmunt, Human TRPA1 is an inherently mechanosensitive bilayer-gated ion channel. *Cell Calcium* **91**, 102255 (2020).
36. A. G. Obukhov, M. C. Nowycky, TRPC5 activation kinetics are modulated by the scaffolding protein ezrin/radixin/moesin-binding phosphoprotein-50 (EBP50). *J. Cell. Physiol.* **201**, 227–235 (2004).
37. A. Gomis, S. Soriano, C. Belmonte, F. Viana, Hypoosmotic- and pressure-induced membrane stretch activate TRPC5 channels. *J. Physiol.* **586**, 5633–5649 (2008).
38. B. Allard, H. Magloire, M. L. Couble, J. C. Maurin, F. Bleicher, Voltage-gated sodium channels confer excitability to human odontoblasts: Possible role in tooth pain transmission. *J. Biol. Chem.* **281**, 29002–29010 (2006).
39. M. R. Byers, Dental sensory receptors. *Int. Rev. Neurobiol.* **25**, 39–94 (1984).
40. H. Ikeda, H. Suda, Odontoblastic syncytium through electrical coupling in the human dental pulp. *J. Dent. Res.* **92**, 371–375 (2013).
41. Y. S. Cho, C. H. Ryu, J. H. Won, H. Vang, S. B. Oh, J. Y. Ro, Y. C. Bae, Rat odontoblasts may use glutamate to signal dentin injury. *Neuroscience* **335**, 54–63 (2016).
42. N. T. Blair, J. S. Kaczmarek, D. E. Clapham, Intracellular calcium strongly potentiates agonist-activated TRPC5 channels. *J. Gen. Physiol.* **133**, 525–546 (2009).
43. P. R. Lee, J. Y. Lee, H. B. Kim, J. H. Lee, S. B. Oh, TRPM8 mediates hyperosmotic stimuli-induced nociception in dental afferents. *J. Dent. Res.* **99**, 107–114 (2019).
44. S. Yamamoto, N. Takahashi, Y. Mori, Chemical physiology of oxidative stress-activated TRPM2 and TRPC5 channels. *Prog. Biophys. Mol. Biol.* **103**, 18–27 (2010).
45. E. K. Curtis, In pursuit of palliation: Oil of cloves in the art of dentistry. *Bull. Hist. Dent.* **38**, 9–14 (1990).
46. P. W. Lucas, S. M. Philip, D. Al-Qeoud, N. Al-Draihim, S. Saji, A. van Casteren, Structure and scale of the mechanics of mammalian dental enamel viewed from an evolutionary perspective. *Evol. Dev.* **18**, 54–61 (2016).

47. K. Y. Kwan, A. J. Allchorne, M. A. Vollrath, A. P. Christensen, D. S. Zhang, C. J. Woolf, D. P. Corey, TRPA1 contributes to cold, mechanical, and chemical Nociception but is not essential for hair-cell transduction. *Neuron* **50**, 277–289 (2006).
48. A. Dhaka, A. N. Murray, J. Mathur, T. J. Earley, M. J. Petrus, A. Patapoutian, TRPM8 is required for cold sensation in mice. *Neuron* **54**, 371–378 (2007).
49. T. Xue, M. T. H. Do, A. Riccio, Z. Jiang, J. Hsieh, H. C. Wang, S. L. Merbs, D. S. Welsbie, T. Yoshioka, P. Weissgerber, S. Stolz, V. Flockerzi, M. Freichel, M. I. Simon, D. E. Clapham, K.-W. Yau, Melanopsin signalling in mammalian iris and retina. *Nature* **479**, 67–73 (2011).
50. I. Vetter, A. Hein, S. Sattler, S. Hessler, F. Touska, E. Bressan, A. Parra, U. Hager, A. Leffler, S. Boukalova, M. Nissen, R. J. Lewis, C. Belmonte, C. Alzheimer, T. Huth, V. Vlachova, P. W. Reeh, K. Zimmermann, Amplified cold transduction in native nociceptors by M-channel inhibition. *J. Neurosci.* **33**, 16627–16641 (2013).
51. I. Vetter, F. Touska, A. Hess, R. Hinsbey, S. Sattler, A. Lampert, M. Sergejeva, A. Sharov, L. S. Collins, M. Eberhardt, M. Engel, P. J. Cabot, J. N. Wood, V. Vlachova, P. W. Reeh, R. J. Lewis, K. Zimmermann, Ciguatoxins activate specific cold pain pathways to elicit burning pain from cooling. *EMBO J.* **31**, 3795–3808 (2012).
52. A. Wyatt, P. Wartenberg, M. Candlish, G. Krasteva-Christ, V. Flockerzi, U. Boehm, Genetic strategies to analyze primary TRP channel-expressing cells in mice. *Cell Calcium* **67**, 91–104 (2017).
53. C. I. Rodriguez, F. Buchholz, J. Galloway, R. Sequerra, J. Kasper, R. Ayala, A. F. Stewart, S. M. Dymecki, High-efficiency deleter mice show that FLPe is an alternative to Cre-*loxP*. *Nat. Genet.* **25**, 139–140 (2000).
54. S. Wen, I. N. Götze, O. Mai, C. Schauer, T. Leinders-Zufall, U. Boehm, Genetic identification of GnRH receptor neurons: A new model for studying neural circuits underlying reproductive physiology in the mouse brain. *Endocrinology* **152**, 1515–1526 (2011).
55. D. C. Hoaglin, B. Iglewicz, Fine-tuning some resistant rules for outlier labeling. *J. Am. Stat. Assoc.* **82**, 1147–1149 (1987).
56. C. Roza, J. A. Lopez-Garcia, Retigabine, the specific KCNQ channel opener, blocks ectopic discharges in axotomized sensory fibres. *Pain* **138**, 537–545 (2008).
57. Y. Matsubayashi, L. Iwai, H. Kawasaki, Fluorescent double-labeling with carbocyanine neuronal tracing and immunohistochemistry using a cholesterol-specific detergent digitonin. *J. Neurosci. Methods* **174**, 71–81 (2008).
58. K. N. Natarajan, Z. Miao, M. Jiang, X. Huang, H. Zhou, J. Xie, C. Wang, S. Qin, Z. Zhao, L. Wu, N. Yang, B. Li, Y. Hou, S. Liu, S. A. Teichmann, Comparative analysis of sequencing technologies for single-cell transcriptomics. *Genome Biol.* **20**, 70 (2019).
59. S. Picelli, A. K. Björklund, O. R. Faridani, S. Sagasser, G. Winberg, R. Sandberg, Smart-seq2 for sensitive full-length transcriptome profiling in single cells. *Nat. Methods* **10**, 1096–1098 (2013).
60. T. D. Wu, S. Nacu, Fast and SNP-tolerant detection of complex variants and splicing in short reads. *Bioinformatics* **26**, 873–881 (2010).
61. Y. Liao, G. K. Smyth, W. Shi, featureCounts: An efficient general purpose program for assigning sequence reads to genomic features. *Bioinformatics* **30**, 923–930 (2014).
62. B. Schmid, P. Tripal, T. Fraass, C. Kersten, B. Ruder, A. Gruneboom, J. Huisken, R. Palmisano, 3Dscript: Animating 3D/4D microscopy data using a natural-language-based syntax. *Nat. Methods* **16**, 278–280 (2019).
63. M. P. Whyte, W. H. McAlister, D. V. Novack, K. L. Clements, P. L. Schoenecker, D. Wenkert, Bisphosphonate-induced osteopetrosis: Novel bone modeling defects, metaphyseal osteopenia, and osteosclerosis fractures after drug exposure ceases. *J. Bone Miner. Res.* **23**, 1698–1707 (2008).
64. J. K. Lennerz, V. Ruhle, E. P. Ceppa, W. L. Neuhuber, N. W. Bunnett, E. F. Grady, K. Messlinger, Calcitonin receptor-like receptor (CLR), receptor activity-modifying protein 1 (RAMP1), and calcitonin gene-related peptide (CGRP) immunoreactivity in the rat trigeminovascular system: Differences between peripheral and central CGRP receptor distribution. *J. Comp. Neurol.* **507**, 1277–1299 (2008).
65. R. A. Colby, *Color Atlas of Oral Pathology; Histology and Embryology, Developmental Disturbances, Diseases of the Teeth and Supporting Structures, Diseases of the Oral Mucosa and Jaws, Neoplasms* (Lippincott Williams & Wilkins, 1961).
66. N. N. Shuhaibar, A. R. Hand, M. Terasaki, Odontoblast processes of the mouse incisor are plates oriented in the direction of growth. *Anat. Rec. (Hoboken)*, 1–8 (2020).

Acknowledgments: We would like to thank A. Reis for access to the Unipick Device, M. Moran and C. Eickmeier for providing HC-070, and M. Engel for HC-030031. J. Schram genotyped the transgenic mice. We thank A. Watson, V. Layton, J. Hardges, O. Crisp, B. Henderson, K. Selle, D. Leahart, K. Keith, and R. Brown for expert technical assistance; G. Krapivinsky, B. Zhou, and J. Li for technical assistance with immunohistochemistry; M. Tripal and B. Schmid for technical assistance with microscopy; M. Isaacs and J. Rossi for scanner and microscope use; H. Liapis and J. Mills for help with antibodies; and numerous helpful discussions with J. S. Lewis, R. Schmidt, and S. El-Mofty. **Funding:** This work was funded by the DFG Heisenberg program (ZI1172/3-1, 3-2, and 4-1), the Interdisciplinary Centre for Clinical Research Erlangen, and the Staedtler Foundation Nürnberg to K.Z.; an FPU Scholarship (FPU15/02262 and EST17/00833, Ministerio de Educación, Cultura y Deporte, Spain) to L.B.; CONICYT 21140372 and MECESUP AUS 1203 fellowships to P.S.-H.; FONDECYT 1191868 and ANID-Millennium Science Initiative Program #NC160011 to S.B.; and DFG funding TRR-152 and SFB 1118 to M.F. and SFB/TR 152 to U.B. **Author contributions:** In 2009, D.E.C., J.K.L., and K.Z. had the idea. K.Z. planned and coordinated the study, involving L.B., C.R., and K.Z. in jaw-nerve model; P.S.-H., S.B., F.T., and K.Z. in calcium imaging; C.K. and K.Z. in behavior; V.S., V.V., K.Z., A.H., and D.E.C. in patch-clamp recordings; L.B., P.S.-H., S.R., and A.D. in transcriptome analysis; Z.W., R.K., P.S.-H., L.B., and C.K. in surgeries; K.Z., Z.W., A.T., A.W., P.W., V.S., L.B., and C.R. in mouse immunohistochemistry and multiphoton microscopy; J.K.L., A.S., and J.D.P. in human teeth immunohistochemistry; M.F. in TRPC5$^{-/-}$; and A.W., F.E., P.W., and U.B. in reporter mice design, generation, and characterization. K.Z., J.K.L., and D.E.C. wrote the manuscript with input from all authors. **Competing interests:** The authors declare that they have no competing interests. **Data and materials availability:** All data needed to evaluate the conclusions in the paper are present in the paper and/or the Supplementary Materials. Additional data related to this paper may be requested from the authors.

Submitted 3 November 2020
Accepted 9 February 2021
Published 26 March 2021
10.1126/sciadv.abf5567

Citation: L. Bernal, P. Sotelo-Hitschfeld, C. König, V. Sinica, A. Wyatt, Z. Winter, A. Hein, F. Touska, S. Reinhardt, A. Tragl, R. Kusuda, P. Wartenberg, A. Sclaroff, J. D. Pfeifer, F. Ectors, A. Dahl, M. Freichel, V. Vlachova, S. Brauchi, C. Roza, U. Boehm, D. E. Clapham, J. K. Lennerz, K. Zimmermann, Odontoblast TRPC5 channels signal cold pain in teeth. *Sci. Adv.* **7**, eabf5567 (2021).

Odontoblast TRPC5 channels signal cold pain in teeth

Laura Bernal, Pamela Sotelo-Hitschfeld, Christine König, Viktor Sinica, Amanda Wyatt, Zoltan Winter, Alexander Hein, Filip Touska, Susanne Reinhardt, Aaron Tragl, Ricardo Kusuda, Philipp Wartenberg, Allen Sclaroff, John D. Pfeifer, Fabien Ectors, Andreas Dahl, Marc Freichel, Viktorie Vlachova, Sebastian Brauchi, Carolina Roza, Ulrich Boehm, David E. Clapham, Jochen K. Lennerz and Katharina Zimmermann

Sci Adv **7** (13), eabf5567.
DOI: 10.1126/sciadv.abf5567